Heitler effect and resonance fluorescence in quantum magnonics

Enes Ilbuğa,[1] V. V. Dobrovitski,[1,2] and Ya. M. Blanter[1]
[1]*Kavli Institute of Nanoscience, Delft University of Technology, Lorentzweg 1, 2628 CJ Delft, The Netherlands*
[2]*QuTech, Delft University of Technology, Lorentzweg 1, 2628 CJ Delft, The Netherlands*

(Received 13 February 2025; revised 3 July 2026; accepted 21 July 2026; published 26 August 2026)

We consider a coupled system of a qubit and a magnon mode in which the qubit is weakly driven. We demonstrate that the spectral steady-state responses of both the qubit and the magnon show, in addition to two sidebands split by the coupling, also a peak at the driving frequency with virtually zero linewidth. This phenomenon, which persists at both strong and weak coupling, is an analog of the Heitler effect in atomic physics and shows the path towards building of coherent magnon sources.

DOI: 10.1103/6cnw-7j94

I. INTRODUCTION

In recent years, magnonics, which studies the properties of magnons—elementary excitations of magnetic structure—has been realized as a potential powerful tool in classical and quantum information transfer [1]. To make it functional, individual magnons need to be controllably excited, manipulated, and detected. Currently, the most common instrument in manipulating magnons is cavity magnonics [2,3]. A magnet is put in a microwave or an optical cavity and interacts with the cavity field via Zeeman and magneto-optical effects. It was first theoretically proposed [4] and then experimentally demonstrated [5,6] that the Zeeman effect leads to a strong coupling of a magnet to the magnetic field of a microwave cavity. This strong coupling became a necessary condition to explore quantum properties of magnons [7] with a perspective of using them for quantum information processing. For example, one of the long-standing problems is quantum state transduction between microwave and optical ranges [8–13], and a recent proposal to use magnons as a part of two-stage transduction [14] requires strong and tunable coupling.

To probe quantum magnons, the experiments add a superconducting transmon qubit to a microwave cavity. In this setup, the role of the cavity is to couple the magnet and the qubit and strong coupling between the two has been achieved [7,15–18]. This scheme is an extension of the circuit QED [19], which is the mainstream architecture for quantum circuits using superconducting qubits. Quantum magnonics is a rapidly developing field, with nontrivial quantum magnonic states already having been demonstrated [20].

There is, however, a significant obstacle towards broad application of magnons in quantum technology. The material of choice is yittirum iron garnet (YIG). This ferrimagnetic insulator has currently the highest available magnetic quality, with the quality factor which can exceed 10^4. At the GHz frequencies, where transmon qubits operate, this means that the lifetime of a magnon is of the order of 100 ns, much below those of a qubit and a cavity. It was theoretically proposed earlier [21–23] that by coupling a magnon directly to a qubit and thus departing from the cavity QED architecture one can facilitate creation of quantum states, but the magnon lifetime still would remain the limiting factor. The quality factor of YIG is a material parameter and currently there are no prospects of increasing it by orders of magnitude [3].

In this work we analyze the possibility to create a long-lived stream of magnons with virtually zero linewidth by implementing a magnonic analog of resonance fluorescence in the Heitler regime [24–27]. This regime was originally discovered and studied for an optical two-level emitter (e.g., atom), weakly driven by a highly monochromatic resonant electromagnetic field (e.g., laser). In such a situation, the incident photons from the driving beam are elastically scattered by the emitter, retaining the frequency and the phase of the driving field. As a result, a stream of indistinguishable single photons is produced, whose frequency and phase are fixed by the driving, such that the linewidth of this component of the emitted radiation is limited only by the degree of monochromaticity of the drive, not by the natural linewidth of the emitter. Such photons have numerous applications in quantum science and technology, for instance, as a valuable resource for quantum communication and entanglement generation.

In this manuscript, we analyze a similar phenomenon for a transmon qubit coupled to a magnonic mode. Other types of qubits are likely to give the same behavior. Unlike the original Heitler's setting [24], where the emitter, besides driving, is coupled to environment (a continuum of electromagnetic modes), we consider a typical magnonic system, where the qubit is strongly coupled to a single magnon mode and both are coupled to their environments, leading to finite lifetimes—γ^{-1} of the qubit and κ^{-1} of the magnon. We demonstrate that if one of the systems is weakly driven, a narrow spectral peak develops in both systems at the frequency of the driving field, with the linewidth limited only by the stability

Published by the American Physical Society under the terms of the Creative Commons Attribution 4.0 International license. Further distribution of this work must maintain attribution to the author(s) and the published article's title, journal citation, and DOI.

of the driving field. The peak has (nominally) zero width, as in the standard quantum-optical Heitler effect, demonstrating that the coherent driving is transformed by the magnon-qubit system into a long-lived (formally, infinitely long-lived, i.e., stationary) stream of single quanta, having practically zero linewidth, which populate a hybrid magnon-qubit mode. Thus highly stable long-lived correlations between the states of the qubit and of the magnonic mode, with the fixed phase and frequency, are established in a stationary state. Such long-lived excitations would be useful for a variety of quantum information tasks, such as high-precision sensing and metrology, or for entangling different qubits [25,28,29]. Besides, we predict the strong coupling regime $g \gg \gamma, \kappa$ which does not appear in the standard quantum-optical setting but can be realized for qubit-magnon coupling at the experimentally achieved coupling of 10 MHz [3,7].

Below, we describe the model and the methods in Sec. II, followed by the discussion of the results, first numerical and then analytical, in both weak and strong coupling limits in Sec. III. We present the conclusions in Sec. IV. In the Appendix, we provide more details of the calculation and discuss the decay spectra of both magnon and qubit.

II. MODEL

We assume that the frequencies of the qubit ω_q and the magnon ω_m are close to each other and that the coupling is linear. The linear coupling can be realized either by using a cavity [3] (in which case we consider the cavity to be integrated out) or directly without a cavity [21]. In both scenarios, the physical origin of the coupling is the Zeeman interaction of the magnetization with the magnetic component of the microwave field. The qubit is described by the Pauli matrices and the magnon mode is considered to be a harmonic oscillator. It is convenient to describe the system in the frame rotating with the frequency of the drive ω_L; this is done by applying a unitary transformation to the original Hamiltonian $\hat{H}'$ and obtaining the transformed Hamiltonian $\hat{H} = \hat{D}\hat{H}'\hat{D}^\dagger + i\dot{\hat{D}}\hat{D}^\dagger$, where the operator $\hat{D} = \exp[i\omega_L t(\hat{\sigma}_z/2 + \hat{m}^\dagger\hat{m})]$; see the Appendix. The secular part of the Hamiltonian in the rotating frame becomes

$$\hat{H} = \tfrac{1}{2}\Delta_q\hat{\sigma}_z + \Delta_m\hat{m}^\dagger\hat{m} + g(\hat{\sigma}_+\hat{m} + \hat{\sigma}_-\hat{m}^\dagger) + \Omega(\hat{\sigma}_+ + \hat{\sigma}_-). \tag{1}$$

Here $\hat{\sigma}_z$, $\hat{\sigma}_+$, and $\hat{\sigma}_-$ are the Pauli spin operators acting on the qubit, $\hat{m}^\dagger$ and $\hat{m}$ are respectively the bosonic magnon creation and annihilation operators, $\Delta_q = \omega_q - \omega_L$ and $\Delta_m = \omega_m - \omega_L$ are the detuning of qubit and magnon frequencies from the driving frequency ω_L, g is the interaction strength, and Ω is the driving strength. The first three terms of the Hamiltonian represent the Jaynes-Cummings model (see Ref. [19]), whereas the last term describes the external drive. For simplicity, the Planck's constant $\hbar$ is set to 1 in this Hamiltonian and subsequent equations. In Eq. (1) we use the rotating wave approximation, which is justified as far as we do not consider the Lamb shift [30].

The dissipation is included using the Markovian master equation in Lindblad representation; the non-Markovian terms do not add any new physics and are negligible in the situation considered here; see Ref. [31]. The master equation reads

$$\frac{d}{dt}\hat{\rho}(t) = i[\hat{\rho}(t), \hat{H}] + \frac{\gamma}{2}(2\hat{\sigma}_-\hat{\rho}(t)\hat{\sigma}_+ - \{\hat{\sigma}_+\hat{\sigma}_-, \hat{\rho}(t)\}) + \frac{\kappa}{2}(2\hat{m}\hat{\rho}(t)\hat{m}^\dagger - \{\hat{m}^\dagger\hat{m}, \hat{\rho}(t)\}), \tag{2}$$

where $\hat{\rho}$ is the density operator in the interaction picture, the square (curly) brackets denote the (anti)commutator, and γ and κ represent the spontaneous emission rates of the qubit and magnon, respectively. In the current quantum magnonics experiments, both magnons and qubits have their frequency in the GHz range and operate at sub-kelvin temperatures, so that the thermally induced emission and absorption can be disregarded.

We are interested in analyzing the spectral steady-state response of the qubit and of the magnonic mode, given by [32]

$$S_q(\omega) = 2\,\mathrm{Re}\int_0^\infty d\tau\, e^{-i(\omega-\omega_L)\tau}\langle\hat{\sigma}_+(\tau)\hat{\sigma}_-(0)\rangle_{\mathrm{ss}}, \tag{3a}$$

$$S_m(\omega) = 2\,\mathrm{Re}\int_0^\infty d\tau\, e^{-i(\omega-\omega_L)\tau}\langle\hat{m}^\dagger(\tau)\hat{m}(0)\rangle_{\mathrm{ss}}, \tag{3b}$$

i.e., by the Fourier transform of the steady-state correlation functions of the qubit $\hat{\sigma}_-(t)$ and the magnon mode $\hat{m}(t)$ operators. The spectra of the correlation functions determine the dynamics of the decay and the response to driving.

III. RESULTS

A typical form of the spectral response functions for the qubit and the magnon is shown in Fig. 1 for the case where the driving is exactly in resonance with both the qubit and the magnon, $\omega_L = \omega_q = \omega_m = \omega_0$. The two side peaks in both $S_q(\omega)$ and $S_m(\omega)$, which arise at the frequencies $\omega_0 \pm g$, correspond to an expected response of two strongly coupled subsystems, with finite peak widths controlled by the respective finite lifetimes γ^{-1} and κ^{-1} of the qubit and the magnon. The peak heights in the qubit and magnon spectra correspond to their respective weights in the hybrid modes of the coupled system. In addition, a central δ-function (zero-width) peak develops at the driving frequency ω_0; this peak is a magnonic analog of the Heitler effect and corresponds to elastic scattering of the driving field by the strongly coupled qubit-magnon system. This δ-like peak is primarily of interest for us, since its width is limited by the very narrow bandwidth of the driving source and is independent of the decay rates of the qubit or the magnon. Note that, in contrast with the conventional Heitler effect in quantum optics, now *both* modes, the qubit and the magnon, exhibit the central peak and the two sideband peaks.

Finding the explicit form for the correlation functions in Eq. (3) requires solution of the master equation (2), which, in general, is a daunting task. However, we are mostly interested in the weak driving regime, where the δ-function peaks are most prominent [33]. Accordingly, we limit ourselves to the subspace consisting of the three states $|0\rangle \equiv |g, 0\rangle$, $|m\rangle \equiv |g, 1\rangle$, and $|q\rangle \equiv |e, 0\rangle$, where g and e are the ground and the excited states of the qubit and 0 and 1 stand for the presence of zero and one magnon, respectively. The occupation of the higher states, $|e, 1\rangle$ and $|g, 2\rangle$, scales with the square

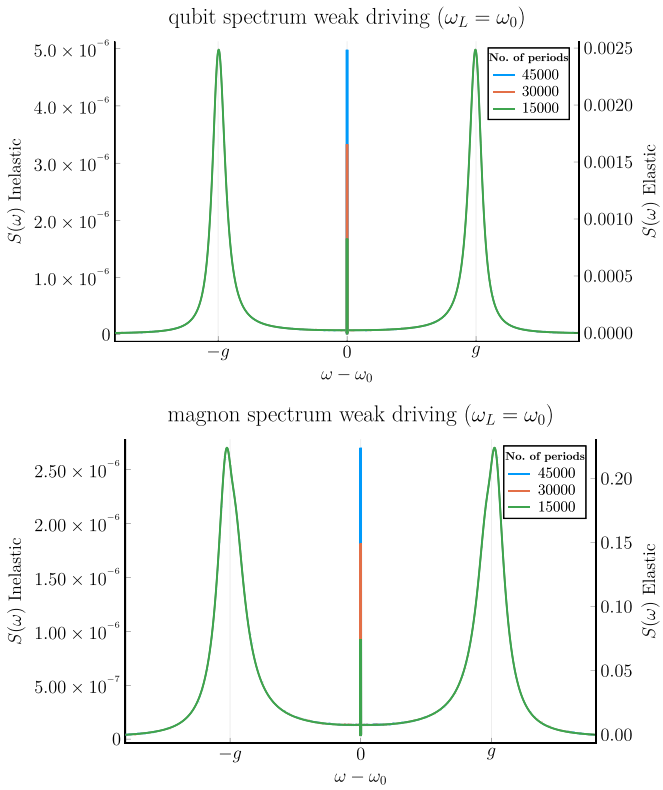


FIG. 1. Qubit (top) and the magnon (bottom) spectrum with a weak external drive. They are plotted for different numbers of time periods upon which the integral is calculated. The parameters are $g = 50$, $\gamma = 5$, $\kappa = 10$, and $\Omega = 1$ (in arbitrary units).

of the driving amplitude and these states can be disregarded. Solution confined to this three-state basis is valid as long as the driving amplitude satisfies $\Omega \ll \gamma$ or $\Omega \ll \kappa$. Writing the master equation in this basis gives us the following set of differential equations:

$$\frac{d}{dt}\langle\hat{m}\rangle = -(i\Delta + \kappa/2)\langle\hat{m}\rangle - ig\langle\hat{\sigma}_-\rangle + i\Omega\langle\hat{\sigma}_+\hat{m}\rangle, \tag{4a}$$

$$\frac{d}{dt}\langle\hat{\sigma}_-\rangle = -(i\Delta + \gamma/2)\langle\hat{\sigma}_-\rangle - ig\langle\hat{m}\rangle + i\Omega(2\langle\hat{\sigma}_+\hat{\sigma}_-\rangle + \langle\hat{m}^\dagger\hat{m}\rangle - 1), \tag{4b}$$

$$\frac{d}{dt}\langle\hat{\sigma}_+\hat{m}\rangle = -\frac{\gamma+\kappa}{2}\langle\hat{\sigma}_+\hat{m}\rangle + ig(\langle\hat{m}^\dagger\hat{m}\rangle - \langle\hat{\sigma}_+\hat{\sigma}_-\rangle) + i\Omega\langle\hat{m}\rangle, \tag{4c}$$

$$\frac{d}{dt}\langle\hat{m}^\dagger\hat{m}\rangle = -\kappa\langle\hat{m}^\dagger\hat{m}\rangle + ig(\langle\hat{\sigma}_+\hat{m}\rangle - \langle\hat{\sigma}_+\hat{m}\rangle^\dagger), \tag{4d}$$

$$\frac{d}{dt}\langle\hat{\sigma}_+\hat{\sigma}_-\rangle = -\gamma\langle\hat{\sigma}_+\hat{\sigma}_-\rangle + ig(\langle\hat{\sigma}_+\hat{m}\rangle^\dagger - \langle\hat{\sigma}_+\hat{m}\rangle) + i\Omega(\langle\hat{\sigma}_-\rangle - \langle\hat{\sigma}_-\rangle^\dagger). \tag{4e}$$

We now consider numerical and analytical solutions of these equations.

A. Numerical integration

We first integrate Eqs. (4a)–(4e) numerically to analyze the effect of driving for various parameter values. Then, using the discrete Fourier transform, as defined in Ref. [34], the spectral distributions [Eqs. (A7b) and ((A7a) are calculated. In Fig. 1 the spectral distributions are plotted at exact resonance ($\omega_q = \omega_m = \omega_L \equiv \omega_0$) in the strong coupling regime ($g \gg \kappa, \gamma$).

As we discussed above, a δ-function-like peak occurs at the driving frequency ω_0 for both the qubit and the magnon, along with two Lorentzian sidebands at $\omega = \omega_0 \pm g$. These sidebands have the same line shape as the decay spectra of the qubit and magnon (see the Appendix). The central peak occurring in both the qubit and magnon spectra is not present in the decay spectra, being the result of driving the qubit. Since we make use of the discrete Fourier transform, the central peak has finite height that scales linearly with the number of time intervals N_t as the total integration time grows, as seen in Fig. 1. Thus the central peak indeed is not Lorentzian, but has a δ-function character. It is important to note that this central peak appears only when the qubit is driven. When the driving stops, the steady-state populations of both the magnon and the qubit modes decay with their characteristic decay rates.

The stationary nonzero values of the correlation functions demonstrate that there are strong long-lived correlations between the states of the qubit and of the magnonic mode, i.e., between the states $|m\rangle \equiv |g, 1\rangle$ and $|q\rangle \equiv |e, 0\rangle$: the mutual phase between these states is locked in the stationary regime and is preserved for the whole duration of driving. Such a state constitutes a useful resource for a variety of quantum information tasks [25,28,29].

B. Analytical solutions

To find the magnitude and characteristics of the peaks, we solve the system of equations analytically in the limit of weak driving. The steady-state solutions for the single time operators $\langle\hat{\sigma}_+\rangle$ and $\langle\hat{m}^\dagger\rangle$ provide us with the magnitudes of the δ functions [33]. These steady-state solutions are readily found by rewriting the differential equations as a matrix equation (see the Appendix). In the weak driving limit they are

$$|\langle\hat{\sigma}_+\rangle_{ss}|^2 = \frac{\Omega^2\left(\Delta^2 + \frac{1}{4}\kappa^2\right)}{g^4 + \Delta^4 + \frac{1}{4}\gamma^2\Delta^2 + \frac{1}{4}\kappa^2\Delta^2 - 2\Delta^2 g^2 + \frac{1}{16}\kappa^2\gamma^2 + \frac{1}{2}g^2\gamma\kappa} \tag{5}$$

and

$$|\langle\hat{m}^\dagger\rangle_{ss}|^2 = \frac{\Omega^2 g^2}{g^4 + \Delta^4 + \frac{1}{4}\gamma^2\Delta^2 + \frac{1}{4}\kappa^2\Delta^2 - 2\Delta^2 g^2 + \frac{1}{16}\kappa^2\gamma^2 + \frac{1}{2}g^2\gamma\kappa}, \tag{6}$$

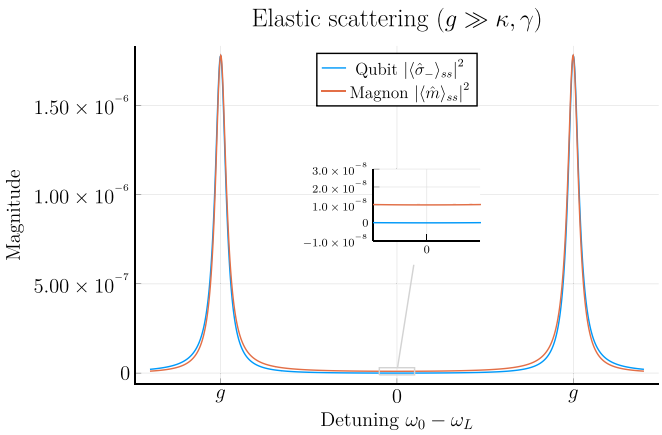


FIG. 2. Elastic scattering amplitude of the qubit and the magnon plotted against the driving frequency in the strong coupling regime. The parameters are $g = 100$, $\Omega = 0.01$, $\gamma = 15$, and $\kappa = 0$ (in arbitrary units).

where $\Delta = \omega_0 - \omega_L$ and $\omega_q = \omega_m \equiv \omega_0$, i.e., the qubit and magnon operate at the same frequency. Equations (A19) and (A20) give us the magnitudes of the δ functions, proportional to the driving strength Ω. These magnitudes will now be considered in different limits.

In the *strong coupling limit* ($g \gg \gamma, \kappa$), Fig. 2 presents a plot of the magnitude of the delta peak in the corresponding spectra for various driving frequencies. We note that the qubit and magnon have almost identical scattering amplitudes. The presence of the magnon magnitude in Fig. 2 verifies that driving the qubit induces elastic scattering of the magnon. The shapes of both magnitudes follow the shape of the decay spectrum (see the Appendix), which is expected in the weak driving regime [24]. Note that the strong coupling regime does not occur in the standard Heitler framework in quantum optics.

For the *weak coupling* ($g \ll \gamma, \kappa$), the elastic scattering magnitude is visualized in Fig. 3. We see that, even in the weak coupling limit, the magnon emission line contains a delta peak, albeit with a much smaller magnitude than that of the qubit. In this limit, the magnon decay spectrum is

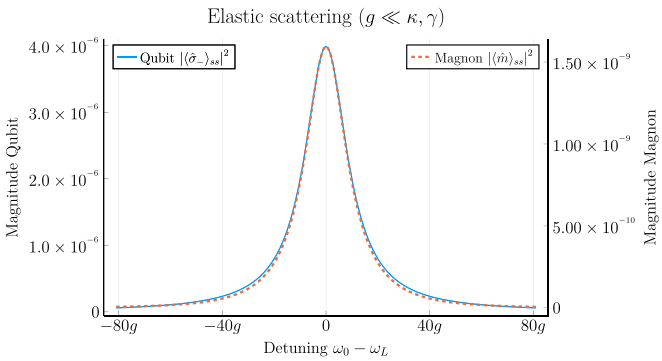


FIG. 3. Elastic scattering magnitude of the qubit and the magnon plotted against the driving frequency in the weak coupling regime. The parameters are $g = 0.5$, $\Omega = 0.01$, $\gamma = 10$, and $\kappa = 50$ (in arbitrary units).

independent of the qubit decay spectrum (see the Appendix). Here however the magnon follows the line shape of the qubit, that is, if the driving is slightly detuned from the resonance frequency but remains within the natural linewidth, then the amplitude of the δ peak is reduced, following the natural shape of the resonance line. Physically one would expect the qubit scattering magnitude to be larger since the magnon "feels" less of the driving because of the weaker coupling strength. The scattering amplitudes at the maximum $\omega_0 = \omega_L$ are

$$|\langle\hat{\sigma}_+\rangle_{ss}|^2 = \frac{4\Omega^2}{\gamma^2}, \quad |\langle\hat{m}^\dagger\rangle_{ss}|^2 = \frac{16\Omega^2 g^2}{\kappa^2\gamma^2}. \tag{7}$$

We see that the qubit scattering magnitude is independent of the decay of the magnon. This is expected since we drive the qubit. At the same time, the magnon peak grows with increasing coupling strength. The magnon peak at the maximum is smaller by a factor of $\kappa^2/(4g^2)$. The corresponding density matrix exhibits that the stationary state consists almost exclusively of a single pure quantum state where all three levels $|g, 0\rangle$, $|g, 1\rangle$, and $|e, 0\rangle$ are hybridized, but the amplitude of the state $|g, 1\rangle$ (magnon excitation) is much smaller than the amplitude of $|e, 0\rangle$ (qubit excitation) due to small magnon-qubit cooperativity in the weak coupling regime. Thus, in experiments, the magnons will decouple from the qubit at long times, in the same way as it happens in optics, where the photon emission happens by forming a hybrid quantum state (involving both atomic and photonic excitations) but the propagating photon at long times decouples from the atom. Such a decoupling, however, is not expected in the strong coupling regime, where the qubit and the magnonic excitations form the symmetric states $|g, 1\rangle \pm |e, 0\rangle$ which are split by a large energy gap $2g$, and only one of these states is excited by the driving (depending on the detuning $\omega_0 - \omega_L$).

IV. CONCLUSIONS

Our predictions can be tested experimentally, for instance, by implementing the strong coupling regime and measuring the delta-function response of the qubit as a function of the driving frequency; the strongest resonant response should occur when the driving frequency is *detuned* from the resonance frequency of the qubit/magnon by the amount $\pm g$ (see Fig. 2) Another possibility is to measure the magnetic response using another qubit (e.g., transmon [3] or a NV center in diamond [35]) as a detector, similar to Refs. [7,15–18]; the magnonic response should demonstrate a delta-function peak along with the "regular" response, having the natural linewidth of a magnon.

In conclusion, we have considered the system of coupled transmon qubit and a magnon mode and found that at weak driving the spectral responses of both the qubit and the magnon develop a narrow delta peak at the driving frequency. This effect is a magnonic analog of the Heitler regime of resonance fluorescence [24] and represents elastic scattering of the driving by the qubit (more precisely, by the strongly coupled system of the qubit and the magnonic mode). As a result, a stationary stream of hybrid magnon-qubit excitations is produced, whose phase and frequency are determined by the driving, with virtually zero linewidth, not limited by the qubit or the magnon lifetimes [36]. At the same time, stable

long-lived correlations between the states of the qubit and of the magnonic mode are established, with the fixed phases between the states $|0\rangle \equiv |g,0\rangle$, $|m\rangle \equiv |g,1\rangle$, and $|q\rangle \equiv |e,0\rangle$. In the weak-coupling regime, the propagating magnons will decouple from the qubit at long times, but in the strong-coupling situation, such a decoupling will not happen, since only one of the states $|g,1\rangle \pm |e,0\rangle$ is excited by driving.

This effect can be a valuable resource for magnon-based quantum sensing and metrology. Besides, the highly stable correlations between the states of the qubit and the magnon mode could be used for entangling different qubits, in analogy to a broad spectrum of entangling protocols developed in quantum optics; see, e.g., Refs. [11–13,28,29,37–39], provided that single magnons are reliably detected with reasonable efficiency.

ACKNOWLEDGMENTS

The work was supported by the Dutch Research Council (NWO). This work is part of the research program NWO QuTech Physics Funding (QTECH, Program 172) with Project No. 16QTECH02, which is (partly) financed by NWO.

DATA AVAILABILITY

There are no publicly available research data or software supporting this manuscript. Requests for further information or data should be sent to the authors.

APPENDIX: DECAY SPECTRA

Our starting point is the Hamiltonian for a qubit resonantly coupled to a single magnon mode, see, e.g., Ref. [3],

$$\hat{H}' = \tfrac{1}{2}\omega_q\hat{\sigma}_z + \omega_m\hat{m}^\dagger\hat{m} + g(\hat{\sigma}_+\hat{m} + \hat{\sigma}_-\hat{m}^\dagger) + \Omega(\hat{\sigma}_+e^{-i\omega_L t} + \hat{\sigma}_-e^{i\omega_L t}), \tag{A1}$$

where $\hat{\sigma}$ are the Pauli operators describing the qubit and $\hat{m}$ is the annihilation operator for the magnon. To derive Eq. (A1), we linearized the Holstein-Primakoff transformation, so that the magnon mode is described as a harmonic oscillator. Furthermore, ω_q and ω_m are the frequencies of the qubit (Rabi frequency) and the magnon, g is the coupling constant, and the last term in Eq. (A1) describes external drive with the amplitude Ω and the frequency ω_L. As in the main text, we use units with $\hbar = 1$.

It is convenient to move to the frame rotating with the frequency of the drive ω_L; this is done by applying a unitary transformation $\hat{H} = \hat{D}\hat{H}'\hat{D}^\dagger + i\dot{\hat{D}}\hat{D}^\dagger$, where the operator $\hat{D} = \exp[i\omega_L t(\hat{\sigma}_z/2 + \hat{m}^\dagger\hat{m})]$. We get the transformed Hamiltonian, Eq. (1),

$$\hat{H} = \tfrac{1}{2}\Delta_q\hat{\sigma}_z + \Delta_m\hat{m}^\dagger\hat{m} + g(\hat{\sigma}_+\hat{m} + \hat{\sigma}_-\hat{m}^\dagger) + \Omega(\hat{\sigma}_+ + \hat{\sigma}_-), \tag{A2}$$

with $\Delta_{q,m} = \omega_{q,m} - \omega_L$. In the following, we assume that the qubit and the magnon are exactly at resonance, $\omega_q = \omega_m = \omega_0$, and define the detuning from the driving frequency $\Delta = \omega_0 - \omega_L$.

To calculate the decay spectra, we disregard the driving and consider the qubit initially in the excited state and the magnon with a population of one. The differential equations describing this system are

$$\frac{d}{dt}\langle\hat{m}^\dagger\rangle = (i\Delta - \kappa/2)\langle\hat{m}^\dagger\rangle + ig\langle\hat{\sigma}_+\rangle, \tag{A3a}$$

$$\frac{d}{dt}\langle\hat{\sigma}_+\rangle = (i\Delta - \gamma/2)\langle\hat{\sigma}_+\rangle + ig\langle\hat{m}^\dagger\rangle, \tag{A3b}$$

where γ and κ are the decay parameters of the qubit and the magnon, respectively. We get the following solutions:

$$\begin{bmatrix}\langle\hat{m}^\dagger\rangle(t)\\ \langle\hat{\sigma}_+\rangle(t)\end{bmatrix} = A\begin{bmatrix}i(\kappa-\gamma)+\mu\\ 4g\end{bmatrix}e^{[-(\gamma+\kappa)+i\mu]t/4} + B\begin{bmatrix}i(\kappa-\gamma)-\mu\\ 4g\end{bmatrix}e^{[-(\gamma+\kappa)-i\mu]t/4}, \tag{A4}$$

where A and B depend on the initial conditions and $\mu = \sqrt{16g^2 - (\gamma-\kappa)^2}$. To calculate the spectra, we first need expressions for the correlation functions $\langle\hat{m}^\dagger(t)\hat{m}(0)\rangle$ and $\langle\hat{\sigma}_+(t)\hat{\sigma}_-(0)\rangle$. By the quantum regression theorem [40], these are given by Eq. (A4) but with $\langle\hat{m}^\dagger(t)\rangle$ and $\langle\hat{\sigma}_+(t)\rangle$ replaced by $\langle\hat{m}^\dagger(t)\hat{m}(0)\rangle$ and $\langle\hat{\sigma}_+(t)\hat{\sigma}_-(0)\rangle$, respectively. Using the initial conditions $\langle\hat{m}^\dagger(0)\hat{m}(0)\rangle = 1$ and $\langle\hat{\sigma}_+(0)\hat{\sigma}_-(0)\rangle = 1$, we obtain the correlation functions

$$\langle\hat{m}^\dagger(t)\hat{m}(0)\rangle = \frac{i(\gamma-\kappa)+\mu}{2\mu}e^{[-(\gamma+\kappa)-i\mu+i\omega_0]t/4} + \frac{i(\kappa-\gamma)+\mu}{2\mu}e^{[-(\gamma+\kappa)+i\mu+i\omega_0]t/4}, \tag{A5}$$

$$\langle\hat{\sigma}_+(t)\hat{\sigma}_-(0)\rangle = \frac{i(\kappa-\gamma)+\mu}{2\mu}e^{[-(\gamma+\kappa)-i\mu+i\omega_0]t/4} + \frac{i(\gamma-\kappa)+\mu}{2\mu}e^{[-(\gamma+\kappa)+i\mu+i\omega_0]t/4}. \tag{A6}$$

Calculating the spectral distribution functions [32]

$$S_m(\omega) = 2\,\mathrm{Re}\int_0^\infty dt\, e^{-i(\omega-\omega_L)t}\langle\hat{m}^\dagger(t)\hat{m}(0)\rangle, \tag{A7a}$$

$$S_q(\omega) = 2\,\mathrm{Re}\int_0^\infty dt\, e^{-i(\omega-\omega_L)t}\langle\hat{\sigma}_+(t)\hat{\sigma}_-(0)\rangle, \tag{A7b}$$

we find the decay spectra,

$$S_m(\omega) = 2\,\mathrm{Re}\left[\frac{i(\gamma-\kappa)+\mu}{2\mu}\frac{1}{\frac{\gamma+\kappa}{4}+i(\omega-\omega_0+\mu/4)} + \frac{i(\kappa-\gamma)+\mu}{2\mu}\frac{1}{\frac{\gamma+\kappa}{4}+i(\omega-\omega_0-\mu/4)}\right], \tag{A8}$$

$$S_q(\omega) = 2\,\mathrm{Re}\left[\frac{i(\kappa-\gamma)+\mu}{2\mu}\frac{1}{\frac{\gamma+\kappa}{4}+i(\omega-\omega_0+\mu/4)} + \frac{i(\gamma-\kappa)+\mu}{2\mu}\frac{1}{\frac{\gamma+\kappa}{4}+i(\omega-\omega_0-\mu/4)}\right]. \tag{A9}$$

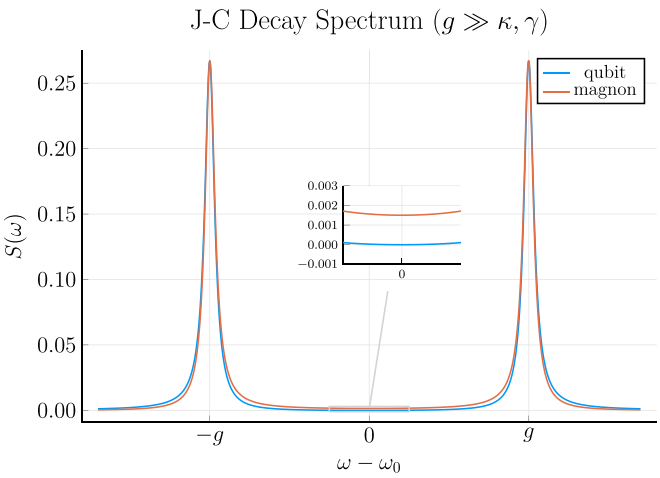


FIG. 4. Decay spectrum of the qubit and the magnon within the Jaynes-Cummings model. Plotted for $g = 100$, $\gamma = 15$, and $\kappa = 0$.

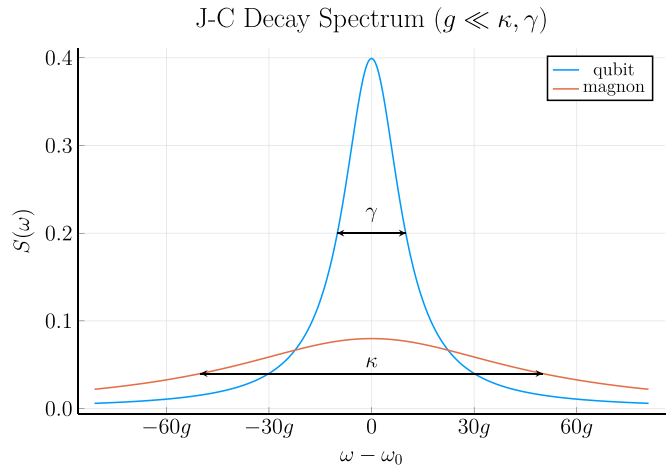


FIG. 5. Decay spectrum of the qubit and the magnon within the Jaynes-Cummings model. Plotted for $g = 0.5$, $\gamma = 10$, and $\kappa = 50$.

These two expressions are similar, but their difference will become apparent when we consider different limits.

1. Strong coupling limit

We start by considering the strong coupling limit, $g \gg \kappa, \gamma$. In this limit, the parameter μ can be approximated as real and equal to $\mu = 4g$. Substituting this value of μ into Eqs. (A8) and (A9) gives us the following two-peak spectra:

$$S_m(\omega) = \frac{-(\gamma-\kappa)(\omega_0-\omega)/4g + \gamma/2}{\left(\frac{\gamma+\kappa}{4}\right)^2 + [\omega - (\omega_0 - g)]^2} + \frac{-(\gamma-\kappa)(\omega-\omega_0)/4g + \gamma/2}{\left(\frac{\gamma+\kappa}{4}\right)^2 + [\omega - (\omega_0 + g)]^2}, \tag{A10}$$

$$S_q(\omega) = \frac{(\gamma-\kappa)(\omega_0-\omega)/4g + \kappa/2}{\left(\frac{\gamma+\kappa}{4}\right)^2 + [\omega - (\omega_0 - g)]^2} + \frac{(\gamma-\kappa)(\omega-\omega_0)/4g + \kappa/2}{\left(\frac{\gamma+\kappa}{4}\right)^2 + [\omega - (\omega_0 + g)]^2}. \tag{A11}$$

In Fig. 4, the qubit and the magnon spectrum are plotted as a function of the frequency ω.

The decay spectra show two peaks centered around the energies $\omega_0 \pm g$, which correspond to the dressed states from the Jaynes Cummings model [41]. The near equivalence of both spectra is due to the fact that both systems "blend" into one system due to their strong interaction. Even without magnon decay ($\kappa = 0$) in Fig. 4, the spectra are still nearly equivalent.

2. Weak coupling limit

In the weak coupling limit, we have $g \ll \kappa, \gamma$. We expect the qubit and magnon to become disentangled in this limit and show independent decay spectra. Taking this limit in Eqs. (A8) and (A9) gives the following spectra:

$$S_m(\omega) = 2\,\mathrm{Re}\left[\frac{1}{\frac{\kappa}{2} + i(\omega - \omega_0)}\right] \tag{A12}$$

and

$$S_q(\omega) = 2\,\mathrm{Re}\left[\frac{1}{\frac{\gamma}{2} + i(\omega - \omega_0)}\right]. \tag{A13}$$

These equations indeed confirm what we would expect physically to occur. The decay spectra are once again plotted in Fig. 5 but now for the weak coupling regime.

a. Analytical solution, elastic scattering

Now, let us consider nonzero driving. The corresponding equations of motions are given by Eqs. (4a)–(4e) of the main text.

The driving term Ω couples the operators $\langle \hat{m} \rangle$ and $\langle \hat{\sigma}_- \rangle$ to the operators $\langle \hat{m}^\dagger \hat{m} \rangle$, $\langle \hat{\sigma}_+ \hat{\sigma}_- \rangle$, and $\langle \hat{\sigma}_+ \hat{m} \rangle$. These equations can once again be put into matrix form. To work with only real variables, we will use the real and imaginary parts of the complex operators instead of the complex variable and its conjugate. So, for example, instead of $\langle \hat{\sigma}_+ \hat{m} \rangle$ and $\langle \hat{\sigma}_+ \hat{m} \rangle^\dagger$, we use $\langle \hat{\sigma}_+ \hat{m} \rangle_R$ and $\langle \hat{\sigma}_+ \hat{m} \rangle_I$. The equations in matrix form are then

$$\frac{d}{dt}\mathbf{v} = \mathbf{A}\mathbf{v} + \mathbf{b}, \tag{A14}$$

where

$$\mathbf{v} = \begin{bmatrix} \langle \hat{m} \rangle_R \\ \langle \hat{m} \rangle_I \\ \langle \hat{\sigma}_- \rangle_R \\ \langle \hat{\sigma}_- \rangle_I \\ \langle \hat{\sigma}_+ \hat{m} \rangle_R \\ \langle \hat{\sigma}_+ \hat{m} \rangle_I \\ \langle \hat{m}^\dagger \hat{m} \rangle \\ \langle \hat{\sigma}_+ \hat{\sigma}_- \rangle \end{bmatrix}, \tag{A15}$$

$$\mathbf{A} = \begin{bmatrix} -\frac{1}{2}\kappa & \Delta & 0 & g & 0 & -\Omega & 0 & 0 \\ -\Delta & -\frac{1}{2}\kappa & -g & 0 & \Omega & 0 & 0 & 0 \\ 0 & g & -\frac{1}{2}\gamma & \Delta & 0 & 0 & 0 & 0 \\ -g & 0 & -\Delta & -\frac{1}{2}\gamma & 0 & 0 & \Omega & 2\Omega \\ 0 & -\Omega & 0 & 0 & -\frac{(\gamma+\kappa)}{2} & 0 & 0 & 0 \\ \Omega & 0 & 0 & 0 & 0 & -\frac{(\gamma+\kappa)}{2} & g & -g \\ 0 & 0 & 0 & 0 & 0 & -2g & -\kappa & 0 \\ 0 & 0 & 0 & -2\Omega & 0 & 2g & 0 & -\gamma \end{bmatrix}, \tag{A16}$$

and

$$\mathbf{b} = \begin{bmatrix} 0 \\ 0 \\ 0 \\ -\Omega \\ 0 \\ 0 \\ 0 \\ 0 \end{bmatrix}. \tag{A17}$$

What we have now is a nonhomogeneous system of first-order differential equations. However, the magnitudes of the δ functions are provided by the steady-state solutions of the single time operators $\langle\hat{\sigma}_-\rangle$ and $\langle\hat{m}\rangle$[33] . These steady-state solutions are then calculated with the formula

$$\mathbf{v}_{ss} = -\mathbf{A}^{-1}\mathbf{b}. \tag{A18}$$

The elastic scattering magnitudes are given by

$$|\langle\hat{\sigma}_-\rangle_{ss}|^2 = \frac{\Omega^2\left(\Delta^2 + \frac{1}{4}\kappa^2\right)}{g^4 + \Delta^4 + \frac{1}{4}\gamma^2\Delta^2 + \frac{1}{4}\kappa^2\Delta^2 - 2\Delta^2 g^2 + \frac{1}{16}\kappa^2\gamma^2 + \frac{1}{2}g^2\gamma\kappa}, \tag{A19}$$

$$|\langle\hat{m}\rangle_{ss}|^2 = \frac{\Omega^2 g^2}{g^4 + \Delta^4 + \frac{1}{4}\gamma^2\Delta^2 + \frac{1}{4}\kappa^2\Delta^2 - 2\Delta^2 g^2 + \frac{1}{16}\kappa^2\gamma^2 + \frac{1}{2}g^2\gamma\kappa}. \tag{A20}$$

[1] A. V. Chumak *et al.*, Advances in magnetics roadmap on spin-wave computing, IEEE Trans. Magn. **58**, 1 (2022).

[2] H. Y. Yuan, Y. Cao, A. Kamra, R. A. Duine, and P. Yan, Quantum magnonics: When magnon spintronics meets quantum information science, Phys. Rep. **965**, 1 (2022).

[3] B. Zare Rameshti, S. Viola Kusminskiy, J. A. Haigh, K. Usami, D. Lachance-Quirion, Y. Nakamura, C.-M. Hu, H. X. Tang, G. E. W. Bauer, and Y. M. Blanter, Cavity magnonics, Phys. Rep. **979**, 1 (2022).

[4] Ö. O. Soykal and M. E. Flatté, Strong field interactions between a nanomagnet and a photonic cavity, Phys. Rev. Lett. **104**, 077202 (2010).

[5] H. Huebl, C. W. Zollitsch, J. Lotze, F. Hocke, M. Greifenstein, A. Marx, R. Gross, and S. T. B. Goennenwein, High cooperativity in coupled microwave resonator ferrimagnetic insulator hybrids, Phys. Rev. Lett. **111**, 127003 (2013).

[6] Y. Tabuchi, S. Ishino, T. Ishikawa, R. Yamazaki, K. Usami, and Y. Nakamura, Hybridizing ferromagnetic magnons and microwave photons in the quantum limit, Phys. Rev. Lett. **113**, 083603 (2014).

[7] Y. Tabuchi, S. Ishino, A. Noguchi, T. Ishikawa, R. Yamazaki, K. Usami, and Y. Nakamura, Coherent coupling between a ferromagnetic magnon and a superconducting qubit, Science **349**, 405 (2015).

[8] N. J. Lambert, A. Rueda, F. Sedlmeir, and H. G. L. Schwefel, Quantum information technologies: Coherent conversion between microwave and optical photons–An overview of physical implementations, Adv. Quantum Technol. **3**, 2070011 (2020).

[9] N. Lauk, N. Sinclair, S. Barzanjeh, J. P. Covey, M. Saffman, M. Spiropulu, and C. Simon, Perspectives on quantum transduction, Quantum Sci. Technol. **5**, 020501 (2020).

[10] D. Awschalom *et al.*, Development of quantum interconnects (QuICs) for next-generation information technologies, Phys. Rev. X Quantum **2**, 017002 (2021).

[11] A. B. Matsko, A. A. Savchenkov, V. S. Ilchenko, D. Seidel, and L. Maleki, On fundamental quantum noises of whispering gallery mode electro-optic modulators, Opt. Express **15**, 17401 (2007).

[12] J. M. Taylor, A. S. Sørensen, C. M. Marcus, and E. S. Polzik, Laser cooling and optical detection of excitations in a *LC* electrical circuit, Phys. Rev. Lett. **107**, 273601 (2011).

[13] M. Winger, T. D. Blasius, T. P. Mayer Alegre, A. H. Safavi-Naeini, S. Meenehan, J. Cohen, S. Stobbe, and O. Painter, A chip-scale integrated cavity-electro-optomechanics platform, Opt. Express **19**, 24905 (2011).

[14] F. Engelhardt, V. A. S. V. Bittencourt, H. Huebl, O. Klein, and S. V. Kusminskiy, Optimal broadband frequency conversion via a magnetomechanical transducer, Phys. Rev. Appl. **18**, 044059 (2022).

[15] Y. Tabuchi, S. Ishino, A. Noguchi, T. Ishikawa, R. Yamazaki, K. Usami, and Y. Nakamura, Quantum magnonics: The magnon meets the superconducting qubit, C. R. Phys. **17**, 729 (2016).

[16] D. Lachance-Quirion, Y. Tabuchi, S. Ishino, A. Noguchi, T. Ishikawa, R. Yamazaki, and Y. Nakamura, Resolving quanta of collective spin excitations in a millimeter-sized ferromagnet, Sci. Adv. **3**, e1603150 (2017).

[17] D. Lachance-Quirion, S. P. Wolski, Y. Tabuchi, S. Kono, K. Usami, and Y. Nakamura, Entanglement-based single-shot detection of a single magnon with a superconducting qubit, Science **367**, 425 (2020).

[18] S. P. Wolski, D. Lachance-Quirion, Y. Tabuchi, S. Kono, A. Noguchi, K. Usami, and Y. Nakamura, Dissipation-based quantum sensing of magnons with a superconducting qubit, Phys. Rev. Lett. **125**, 117701 (2020).

[19] A. Blais, A. L. Grimsmo, S. M. Girvin, and A. Wallraff, Circuit quantum electrodynamics, Rev. Mod. Phys. **93**, 025005 (2021).

[20] D. Xu, X.-K Gu, H.-K. Li, Y.-C. Weng, Y.-P. Wang, J. Li, H. Wang, S.-Y. Zhu, and J. Q. You, Quantum control of a single magnon in a macroscopic spin system, Phys. Rev. Lett. **130**, 193603 (2023).

[21] M. Kounalakis, G. E. W. Bauer, and Y. M. Blanter, Analog quantum control of magnonic cat states on a chip by a superconducting qubit, Phys. Rev. Lett. **129**, 037205 (2022).

[22] M. Kounalakis, S. Viola Kusminskiy, and Y. M. Blanter, Engineering entangled coherent states of magnons and phonons via a transmon qubit, Phys. Rev. B **108**, 224416 (2023).

[23] M. Dols, S. Sharma, L. Bechara, Y. M. Blanter, M. Kounalakis, and S. Viola Kusminskiy, Magnon-mediated quantum gates for superconducting qubits, Phys. Rev. B **110**, 104416 (2024).

[24] W. Heitler, *The Quantum Theory of Radiation* (Courier Corporation, Boston, 1984).

[25] C. Matthiesen, A. N. Vamivakas, and M. Atatüre, Subnatural linewidth single photons from a quantum dot, Phys. Rev. Lett. **108**, 093602 (2012).

[26] C. Matthiesen, M. Geller, C. H. H. Schulte, C. Le Gall, J. Hansom, Z. Li, M. Hugues, E. Clarke, and M. Atatüre, Phase-locked indistinguishable photons with synthesized waveforms from a solid-state source, Nat. Commun. **4**, 1600 (2014).

[27] Y. He, Y.-M. He, J. Liu, Y.-J. Wei, H. Y. Ramírez, M. Atatüre, C. Schneider, M. Kamp, S. Höfling, C.-Y. Lu, and J.-W. Pan, Dynamically controlled resonance fluorescence spectra from a doubly dressed single InGaAs quantum dot, Phys. Rev. Lett. **114**, 097402 (2015).

[28] H. K. C. Beukers, M. Pasini, H. Choi, D. Englund, R. Hanson, and J. Borregaard, Remote-entanglement protocols for stationary qubits with photonic interfaces, PRX Quantum **5**, 010202 (2024).

[29] L. I. Childress, J. M. Taylor, A. Sørensen, and M. D. Lukin, Fault-tolerant quantum repeaters with minimal physical resources and implementations based on single-photon emitters, Phys. Rev. A **72**, 052330 (2005).

[30] Z.-H. Li, D.-W. Wang, H. Zheng, S.-Y. Zhu, and M. S. Zubairy, Effect of the counterrotating-wave terms on the spontaneous emission from a multilevel atom, Phys. Rev. A **80**, 023801 (2009).

[31] K. Wodkiewicz and J. H. Eberly, Markovian and non-Markovian behavior in two-level atom fluorescence, Ann. Phys. (N.Y.) **101**, 574 (1976).

[32] M. Scully and M. Zubairy, *Quantum Optics* (Cambridge University Press, Cambridge, UK, 1997).

[33] C. Cohen-Tannoudji, J. Dupont-Roc, and G. Grynberg, *Atom-photon Interactions: Basic Processes and Applications* (John Wiley & Sons, New York, 1998).

[34] M. Newman, *Computational Physics* (CreateSpace Independent Publishing Platform, 2013).

[35] F. Casola, T. van der Sar, and A. Yacoby, Probing condensed matter physics with magnetometry based on nitrogen-vacancy centres in diamond, Nat. Rev. Mater. **3**, 17088 (2018).

[36] Current microwave state-of-the-art sources can provide the driving with the frequency drift less than 10^{-16} Hz over the time span of 1 s; see Ref. [42]. Before this limit is reached, the width of the central peak will be of the order of $1/t_{\mathrm{dr}}$, where t_{dr} is the total driving time.

[37] M. Atatüre, D. Englund, N. Vamivakas, S.-Y. Lee, and J. Wrachtrup, Material platforms for spin-based photonic quantum technologies, Nat. Rev. Mater. **3**, 38 (2018).

[38] L. Tian and H. Wang,Optical wavelength conversion of quantum states with optomechanics, Phys. Rev. A **82**, 053806 (2010).

[39] M. Tsang, Cavity quantum electro-optics. II. Input-output relations between traveling optical and microwave fields, Phys. Rev. A **84**, 043845 (2011).

[40] H. Carmichael, *Statistical Methods in Quantum Optics 1: Master Equations and Fokker-Planck Equations, Physics and Astronomy Online Library* (Springer, Berlin, 1999).

[41] C. Gerry, P. Knight, and P. L. Knight, *Introductory Quantum Optics* (Cambridge University Press, Cambridge, UK, 2005).

[42] T. Nakamura, *et al.*, Coherent optical clock down-conversion for microwave frequencies with 10^{-18} instability, Science **368**, 889 (2020).